Supplementary Material

Measurement of dilational modulus of an adsorbed BSA film using pendant bubble tensiometry: from a clean interface to saturation

Siam Hussain,[a] Johann Eduardo Maradiaga Rivas,[a] Wen-Chi Tseng,[a]
Ruey-Yug Tsay,[b] Boris Noskov,[c] Giuseppe Loglio,[d] and Shi-Yow Lin[a]*

[a] Department of Chemical Engineering, National Taiwan University of Science and Technology, 43, Sec. 4, Keelung Road, Taipei, 106 Taiwan

[b] Department of Biomedical Engineering, National Yang-Ming Chiao Tung University, 155, Sec. 2, Linong St, Taipei, 112 Taiwan

[c] Department of Colloid Chemistry, St. Petersburg State University, Universitetsky pr. 26, 198504 St. Petersburg, Russia

[d] Italian National Research Council – CNR, Institute of Condensed Matter Chemistry and Technologies for Energy, 16149 Genoa, Italy

*Author to whom correspondence should be addressed.

Tel: +886-2-2737-6648, fax: +886-2-2737-6644, e-mail: sylin@mail.ntust.edu.tw

Declarations of interest: none

S1. Literature Review

The physicochemical and rheological properties of protein films at an air-water interface have been extensively studied because of their widespread applicability. The findings from relevant literature (e.g., ref. [14–20]) showed that these properties are generally controlled by the intrinsic stability of the protein molecule, amino acid composition, and molecular conformation. In addition, ref. [14–20] reported that forming a stable/saturated film required significant time. For instance, Dickinson et al. [15] observed that the steady-state shear stress for a β-lactoglobulin (BLG) film was not attained even after 80 hours of equilibration. For the reader's convenience, the findings in ref. [14-20] are further detailed in Table S1.

Table S1. A literature review – key findings in studies investigating the physicochemical and rheological properties of protein films at an air-water interface.

Year 1st author	protein [a]	instrument [b]	Key findings and proposed explanation [c]
1995 Atkinson [14]	BLG	neutron reflectivity	• The structure of an adsorbed BLG film was time-dependent, as evidenced by temporal changes in the neutron reflectivity data over a span of ~5 hrs. • The time-dependent changes were likely due to the rearrangement of the tertiary structure (breakage/reformation of intra-molecular disulphide bonds).
1999 Dickinson [15]	BLG	torsion wire viscometer	• The steady-state value of interfacial shear stress (σ_{ss}) was not attained even after 80 hours of equilibration. • The slow conformational changes and network formation amongst the adsorbed BLG molecules hindered the formation of a stable adsorbed film.
2002 Renault [16]	OVA	IRRAS	• The intensity of IRRAS spectra of an adsorbed OVA film exhibited a notable increase over a duration of 5 – 8 hours. • The continual changes in spectral intensity hinted at the formation of a '2D-cohesive network' (caused by conformational changes amidst adsorbed molecules).
2003 Postel [17]	LYS	X-ray reflectivity	• The intensity of reflected X-rays exhibited sudden time-scale shifts over 24 hours (shifts that were observable beyond the measurement timeframe). • The shifts were attributable to various surface relaxation processes (e.g., network formation), which indicated that the LYS film was yet to reach equilibrium.
2005 Martin [18]	BLG	Couette viscometer	• The interfacial shear stress (σ_{ss}) of an adsorbed BLG film exhibited a continual/near monotonic increase even after a duration of 8 hours. • This continual increase was likely indicative of changes to the structure of BLG film.
2014 Varvara [19]	OVA, BLG	rheometer	• The interfacial shear viscosity (μ_s) of adsorbed OVA and BLG films reached a stable value only after 20 – 30 hrs of equilibration. • The considerable time needed for forming a 'fully developed adsorbed film' was resultant from the slow conformational changes and network formation.
2020 Strazdaite [20]	LYS	VSFG spectroscopy	• The intensity of VSFG spectra continued to increase, even 80-130 hours after the film began to form (despite the ST remaining nearly constant) • The temporal increase in VSFG spectral intensity was resultant from the slow conformational changes and network formation of adsorbed molecules.

[a] BLG – β-lactoglobulin; OVA – ovalbumin; LYS – lysozyme

[b] IRRAS – infrared reflection absorption spectroscopy; VSFG – vibrational sum frequency generation spectroscopy

[c] conformational changes – unfolding of the adsorbed molecules as well as rearrangement of their secondary structure; intrinsic stability - the ability of a protein to maintain its native, functional conformation under a range of conditions;

A literature review, comparing the experimental conditions of studies investigating the dilational rheology of globular protein films [BSA, BLG, ovalbumin (OVA), lysozyme (LYS), human serum albumin (HSA); Tables S2a-e], revealed significant variations in the film's lifetime when *E* was measured. Despite this variation, the measurement duration (lifetime of protein film, t_{life}) could be roughly classified: (i) t = ~24 hrs, (ii) t = 3 – 6, (iii) t = 1 – 3, and (iv) t ≤ 1 hr; as shown in Table S3. The large variation in t_{life} likely indicated that the reported *E* values might correspond to different states of the adsorbed film but not that of a saturated film, particularly those *E* measured at short t_{life}. Note that, there is no answer in the literature on how long it takes for an adsorbed film to reach its saturated state.

Table S2a. A comparison of the experimental conditions in studies investigating the dilational rheology of adsorbed BLG films at an air-water interface.

Year 1st Author	1996 Pittia [48]	1999 Wustneck [49]	2009 Noskov [50]	2017 Ulaganathan [51]
concentration (10^{-10} mol/cm^3)	2700	1 – 100	5	0.05, 0.1
Method	oscillating ring	oscillating drop	oscillating ring	oscillating bubble
oscillation frequency (Hz) [a]	n/a	0.1	n/a	0.2
oscillation amplitude (%) [b]	6-7	10	5	7
duration of each perturbance (s)	n/a	160	10	~25
t_{life} [c]	t = 3, 5, 10, 15, 20, 30, 40 min	t = 1 – 2 hr (10 min intervals)	t = 10 min – 1hr (10 min intervals) t = 1 – 4.5 hr (30 min intervals)	t = 30 s – 18 min (~1.5 min intervals) t = 18 min – 22 hr (~16 min intervals)

[a] oscillation frequency (*f*) – 1/T; where T is the duration of an interfacial perturbance

[b] oscillation amplitude – $\Delta A/A_0$: ΔA = change in SA during an perturbance, and A_0 = SA at the onset of an interfacial perturbance

[c] t_{life} – the specific time when *E* was measured (during the lifetime of an adsorbed film)

Table S2b. A comparison of the experimental conditions in studies investigating the dilational rheology of adsorbed BSA films at an air-water interface.

Year 1st Author	1998 Benjamins [42]	2003 Pereira [43]	2007 Berthold [44]	2010 Noskov [45]	2019 Yang [46]	2020 Milyaeva [47]
concentration (10^{-10} mol/cm^3)	0.15, 0.75, 1.5	15	0.5	0.3	1.5	5
method	oscillating barrier	oscillating bubble	oscillating drop	oscillating barrier	oscillating drop	oscillating ring
oscillation frequency (Hz) [a]	0.013 and 0.13	0.01 – 0.2	0.1	0.1	0.1	0.1
oscillation amplitude (%) [b]	7	4.5	10	3	10	7
duration of each perturbance (s)	n/a	360	10	10	50	n/a
t_{life} [c]	t=1.4, 2.4, 3.3, 4.3, 24 hr	t = 10 min – 3 hr *(after every 20 min interval)* t = 3 – 24 hr *(1-hour intervals)*	t=10 min - 3 hr *(10 min intervals)*	t=10 min -2 hr *(10 min intervals)* t = 2 – 4.5 hr *(30 min intervals*	t =4 min -1.3 hr *(5 min intervals)*	t = 10 min – 2 hr *(10 min intervals)* t = 1.5 – 6 hr *(30 min intervals)*

[a] oscillation frequency (f) – 1/T; where T is the duration of an interfacial perturbance

[b] oscillation amplitude – $\Delta A/A_0$: ΔA = change in SA during an perturbance, and A_0 = SA at the onset of an interfacial perturbance

[c] t_{life} – the specific time when E was measured (during the lifetime of an adsorbed film)

Table S2c. A comparison of the experimental conditions in studies investigating the dilational rheology of adsorbed HSA films at an air-water interface

Year 1st Author	2000 Miller [59]	2018 Fainerman [60]	2018 Kovalchuk [61]
concentration (10^{-10} mol/cm^3)	5	0.5 – 10	n/a
method	oscillating drop	oscillating drop	oscillating drop
oscillation frequency (Hz) [a]	0.1	0.1	0.1
oscillation amplitude (%) [b]	5 - 10	3 - 9	3, 10
duration of each perturbance (s)	3-5	~50	~50
t_{life} [c]	t = 1.6 – 3 hr (10/30 min intervals)	t = 3, 7, 30, and 90 min	t = 3, 7, 30, and 90 min

[a] oscillation frequency (f) – 1/T; where T is the duration of an interfacial perturbance

[b] oscillation amplitude – $\Delta A/A_0$: ΔA = change in SA during a perturbance, and A_0 = SA at the onset of an interfacial perturbance

[c] t_{life}– the specific time when E was measured (during the lifetime of an adsorbed film)

Table S2d. A comparison of the experimental conditions in studies investigating the dilational rheology of adsorbed LYS films at an air-water interface.

Year 1st Author	2014 Delahaije [55]	2015 Milyaeva [56]	2015 Tihonov [57]	2017 Benarouche [58]
concentration (10^{-10} mol/cm^3)	7 – 7000	35	n/a	240
method	oscillating drop	oscillating barrier	oscillating barrier	oscillating bubble
oscillation frequency (Hz) [a]	0.1	0.1	n/a	0.1
oscillation amplitude (%) [b]	5	5	10	25
duration of each perturbance (s)	50	n/a	n/a	n/a
t_{life} [c]	t = 2 min – 1 hr (~2 min intervals)	t = 10 min – 1.5 hr (10 min intervals) t = 1.5 – 5 hr (30 min intervals)	t = 10 min – 1.5 hr (10 min intervals) t = 1.5 – 4.2 hr (30 min intervals)	t = 0.01 – 2

[a] oscillation frequency (f) – 1/T; where T is the duration of an interfacial perturbance

[b] oscillation amplitude – $\Delta A/A_0$: ΔA = change in SA during a perturbance, and A_0 = SA at the onset of an interfacial perturbance

[c] t_{life} – the specific time when E was measured (during the lifetime of an adsorbed film)

Table S2e. A comparison of the experimental conditions in studies investigating the dilational rheology of adsorbed OVA films at an air-water interface.

Year 1st Author	1998 Benjamins [42]	2005 Wierenga [52]	2019 Xiong [53]	2019 Delahaije [54]
concentration (10^{-10} mol/cm^3)	0.15, 0.75, 1.5	22.2	11	11 - 1111
method	oscillating barrier	oscillating bubble	oscillating bubble	oscillating drop
oscillation frequency (Hz) [a]	0.013 and 0.13	n/a	0.1	0.1
oscillation amplitude (%) [b]	7	10	10	5
duration of each perturbance (s)	n/a	10	n/a	50
t_{life} [c]	t = 0.5, 1.4, 2.4, 3.3, 4.3, 24 hr	t = 10 min – 1.4 hr (~10 min intervals)	t = 2 min – 3 hr (10 min intervals)	t = 2 min – 1 hr (~2 min intervals)

[a] oscillation frequency (f) – 1/T; where T is the duration of an interfacial perturbance

[b] oscillation amplitude – $\Delta A/A_0$: ΔA = change in SA during a perturbance, and A_0 = SA at the onset of an interfacial perturbance

[c] t_{life} – the specific time when E was measured (during the lifetime of an adsorbed film)

Table S3. A comparison of t_{life} amongst studies [42-61] investigating adsorbed globular protein films at an air-water interface

t_{life} [a] classification	protein [b]	Year, 1st author	t_{life} [a]
~ 24 hr	BLG	2017 Ulaganathan [51]	t = 0.01 – 22
	BSA	1998 Benjamins [42]	t = 1 – 24
		2003 Pereira [43]	t = 0.2 – 24
	OVA	1998 Benjamins [42]	t = 1 – 24
3 – 6 hr	BLG	2009 Noskov [50]	t = 0.2 – 5
	BSA	2010 Noskov [45]	t = 0.2 – 6
		2020 Milyaeva [47]	t = 0.1 – 6
	LYS	2014 Milyaeva [56]	t = 0.2 – 5
		2015 Tihonov [57]	t = 0.2 – 4
1 – 3 hr	BSA	2007 Berthold [44]	t = 0.2 – 3
	HSA	2018 Fainerman [60]	t = 0.05 – 2
		2018 Kovalcuk [61]	
	LYS	2017 Benarouche [58]	t = 0.01 – 2
	OVA	2019 Xiong [53]	t = 0.05 – 3
≤ 1 hr	BLG	1996 Pittia [48]	t = 0.05 – 0.7
		1999 Wustneck [49]	t = 1 – 2
	BSA	2018 Yang [46]	t = 0.1 – 1
	HSA	2000 Miller [18]	t = 1 – 2
	LYS	2014 Delahaije [55]	t = 0.05 – 1
	OVA	2005 Wierenga [52]	t = 0.2 – 1
		2019 Delahaije [55]	t = 0.05 – 1

[a] t_{life} – the specific time when E was measured (during the lifetime of an adsorbed film)

[b] BLG – β-lactoglobulin; BSA – bovine serum albumin; HSA – human serum albumin; LYS – lysozyme; OVA – ovalbumin;

References

[42] J. Benjamins, E.H. Lucassen-Reynders, Surface dilational rheology of proteins adsorbed at air/water and oil/water interfaces, in: D. Mobius, R. Miller (Eds.), Proteins at Liquid Interfaces, Elsevier, 1998: pp. 341–384.

[43] Pereira, L.G.C.; Théodoly, O.; Blanch, H.W.; Radke, C.J. Dilatational Rheology of BSA Conformers at the Air/Water Interface. *Langmuir* **2003**, *19*, 2349–2356, https://doi.org/10.1021/la020720e.

[44] Berthold, A.; Schubert, H.; Brandes, N.; Kroh, L.; Miller, R. Behaviour of BSA and of BSA-derivatives at the air/water interface. *Colloids Surfaces A: Physicochem. Eng. Asp.* **2007**, *301*, 16–22, https://doi.org/10.1016/j.colsurfa.2006.11.054.

[45] Noskov, B.A.; Mikhailovskaya, A.A.; Lin, S.-Y.; Loglio, G.; Miller, R. Bovine Serum Albumin Unfolding at the Air/Water Interface as Studied by Dilational Surface Rheology. *Langmuir* **2010**, *26*, 17225–17231, https://doi.org/10.1021/la103360h.

[46] Yang, J.; Yu, K.; Tsuji, T.; Jha, R.; Zuo, Y.Y. Determining the surface dilational rheology of surfactant and protein films with a droplet waveform generator. *J. Colloid Interface Sci.* **2018**, *537*, 547–553, https://doi.org/10.1016/j.jcis.2018.11.054.

[47] Milyaeva, O.Y. Dynamic Surface Properties of Solutions of Bovine Serum Albumin Complexes with Silica Nanoparticles. *Colloid J.* **2020**, *82*, 538–545, https://doi.org/10.1134/s1061933x20050117.

[48] Pittia, P.; Wilde, P.J.; Husband, F.A.; Clark, D.C. Functional and Structural Properties of ?-lactoglobulin as Affected by High Pressure Treatment. *J. Food Sci.* **1996**, *61*, 1123–1128, https://doi.org/10.1111/j.1365-2621.1996.tb10944.x.

[49] Wüstneck, R.; Moser, B.; Muschiolik, G. Interfacial dilational behaviour of adsorbed β-lactoglobulin layers at the different fluid interfaces. *Colloids Surfaces B: Biointerfaces* **1999**, *15*, 263–273, https://doi.org/10.1016/s0927-7765(99)00093-4.

[50] Noskov, B.A.; Grigoriev, D.O.; Latnikova, A.V.; Lin, S.-Y.; Loglio, G.; Miller, R. Impact of Globule Unfolding on Dilational Viscoelasticity of β-Lactoglobulin Adsorption Layers. *J. Phys. Chem. B* **2009**, *113*, 13398–13404, https://doi.org/10.1021/jp905413q.

[51] V. Ulaganathan, I. Retzlaff, J.Y. Won, G. Gochev, D.Z. Gunes, C. Gehin-Delval, M. Leser, B.A. Noskov, R. Miller, β-Lactoglobulin adsorption layers at the water/air surface: 2. Dilational rheology: Effect of pH and ionic strength, Colloids Surf A Physicochem Eng Asp. 521 (2017) 167–176.

[52] Wierenga, P.A.; Meinders, M.B.J.; Egmond, M.R.; Voragen, A.G.J.; de Jongh, H.H.J. Quantitative Description of the Relation between Protein Net Charge and Protein Adsorption to Air−Water Interfaces. *J. Phys. Chem. B* **2005**, *109*, 16946–16952, https://doi.org/10.1021/jp050990g.

[53] Xiong, W.; Li, J.; Li, B.; Wang, L. Physicochemical properties and interfacial dilatational rheological behavior at air-water interface of high intensity ultrasound modified ovalbumin: Effect of ionic strength. *Food Hydrocoll.* **2019**, *97*, 105210, https://doi.org/10.1016/j.foodhyd.2019.105210.

[54] Delahaije, R.J.; Lech, F.J.; Wierenga, P.A. Investigating the effect of temperature on the formation and stabilization of ovalbumin foams. *Food Hydrocoll.* **2019**, *91*, 263–274, https://doi.org/10.1016/j.foodhyd.2019.01.030.

[55] Delahaije, R.J.; Gruppen, H.; Giuseppin, M.L.; Wierenga, P.A. Quantitative description of the parameters affecting the adsorption behaviour of globular proteins. *Colloids Surfaces B: Biointerfaces* **2014**, *123*, 199–206, https://doi.org/10.1016/j.colsurfb.2014.09.015.

[56] Milyaeva, O.Y.; Campbell, R.A.; Lin, S.-Y.; Loglio, G.; Miller, R.; Tihonov, M.M.; Varga, I.; Volkova, A.V.; Noskov, B.A. Synergetic effect of sodium polystyrene sulfonate and guanidine hydrochloride on the surface properties of lysozyme solutions. *RSC Adv.* **2014**, *5*, 7413–7422, https://doi.org/10.1039/c4ra14330b.

[57] Tihonov, M.; Milyaeva, O.; Noskov, B. Dynamic surface properties of lysozyme solutions. Impact of urea and guanidine hydrochloride. *Colloids Surfaces B: Biointerfaces* **2015**, *129*, 114–120, https://doi.org/10.1016/j.colsurfb.2015.03.034.

[58] A. Bénarouche, J. Habchi, A. Cagna, O. Maniti, A. Girard-Egrot, J.F. Cavalier, S. Longhi, F. Carrière, Interfacial properties of NTAIL, an intrinsically disordered protein, Biophys J. 113 (2017) 2723–2735.

[59] Miller, R.; Fainerman, V.; Makievski, A.; Krägel, J.; Grigoriev, D.; Kazakov, V.; Sinyachenko, O. Dynamics of protein and mixed protein/surfactant adsorption layers at the water/fluid interface. *Adv. Colloid Interface Sci.* **2000**, *86*, 39–82, https://doi.org/10.1016/s0001-8686(00)00032-4.

[60] Fainerman, V.B.; Kovalchuk, V.I.; Aksenenko, E.V.; Zinkovych, I.I.; Makievski, A.V.; Nikolenko, M.V.; Miller, R. Dilational Viscoelasticity of Proteins Solutions in Dynamic Conditions. *Langmuir* **2018**, *34*, 6678–6686, https://doi.org/10.1021/acs.langmuir.8b00631.

[61] Kovalchuk, V.I.; Aksenenko, E.V.; Trukhin, D.V.; Makievski, A.V.; Fainerman, V.B.; Miller, R. Effect of Amplitude on the Surface Dilational Visco-Elasticity of Protein Solutions. *Colloids Interfaces* **2018**, *2*, 57, https://doi.org/10.3390/colloids2040057.

S2. Relaxations of surface tension (ST) and surface area (SA)

Figure S1a illustrates the relaxations of ST and SA for $C_{BSA} = 15\times10^{-10}$ mol/cm^3. During the first few hours, the ST exhibited a relatively smooth and considerable decrease (from 72 mN/m). Afterward, at t > ~10 hr, the ST relaxed slowly, then eventually reached and remained essentially constant (at ~52.2 mN/m) while exhibiting prominent and sustained fluctuations (Figure 1b). These ST fluctuations were generally observed to be in harmony with the minute variations in SA. Figures S1b and S1c show two examples of these near-synchronized fluctuations in ST and SA at t = 8 – 12 (10^4 s) and t = 21 – 23 (10^4 s), respectively.

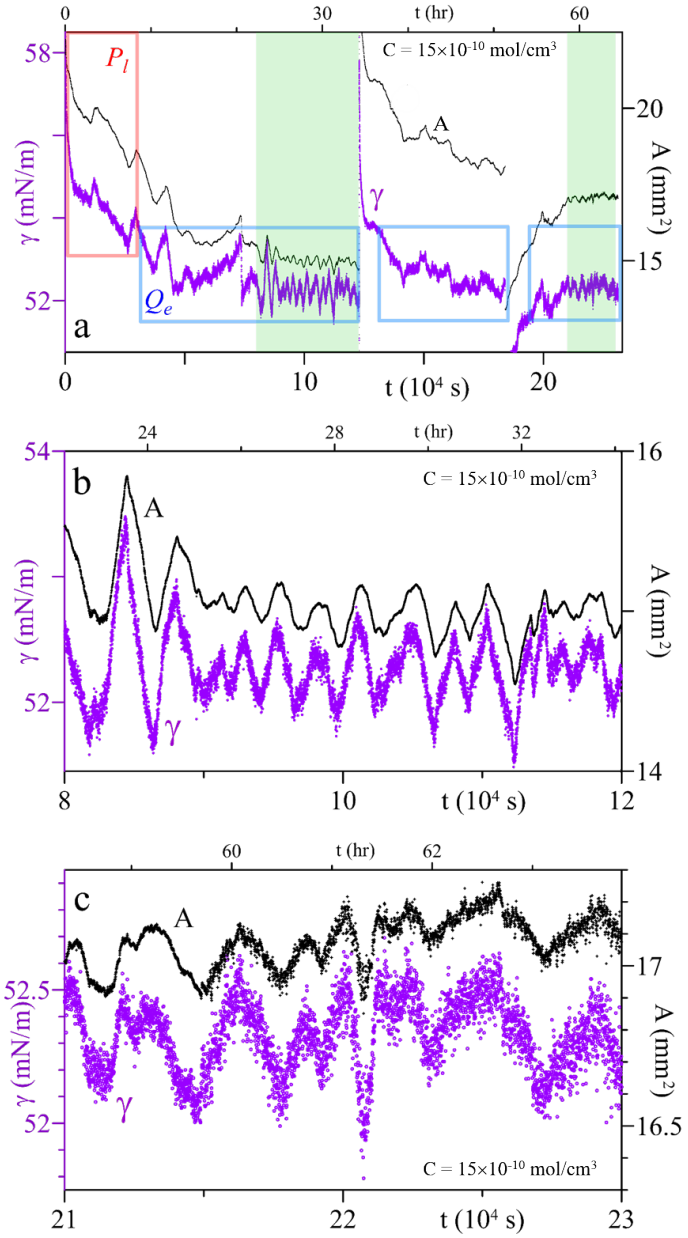

Figure S1. (a) Relaxations of surface tension (γ) and surface area (A) of purely aqueous BSA solution ($C = 15\times10^{-10}$ mol/cm^3) and the pendant bubble, respectively, showing two examples of the near-synchronized fluctuations in ST and SA at the quasi-equilibrium regime (b.c). P_l and Q_e indicate post-induction (latter) and quasi-equilibrium regimes, respectively.

Figure S2a-b illustrates the relaxations of ST and SA for $C_{BSA} = 0.4\times10^{-10}$ mol/cm^3. The ST initially remained nearly constant (at ~72 mN/m, at t < ~0.3 hr) before decreasing smoothly and gradually over the next six hours or so. Meanwhile, the SA remained fairly constant at t < ~0.2 hr (±1.4% variation, Figure S2a); then decreased steadily (t < ~0.3 hr). Afterward (at t > ~6 hr), the ST relaxed slowly, then eventually reached and remained essentially constant (at ~52.2 mN/m) while exhibiting prominent and sustained fluctuations (Figure S2b). These ST fluctuations were generally observed to be in harmony with the minute variations in SA

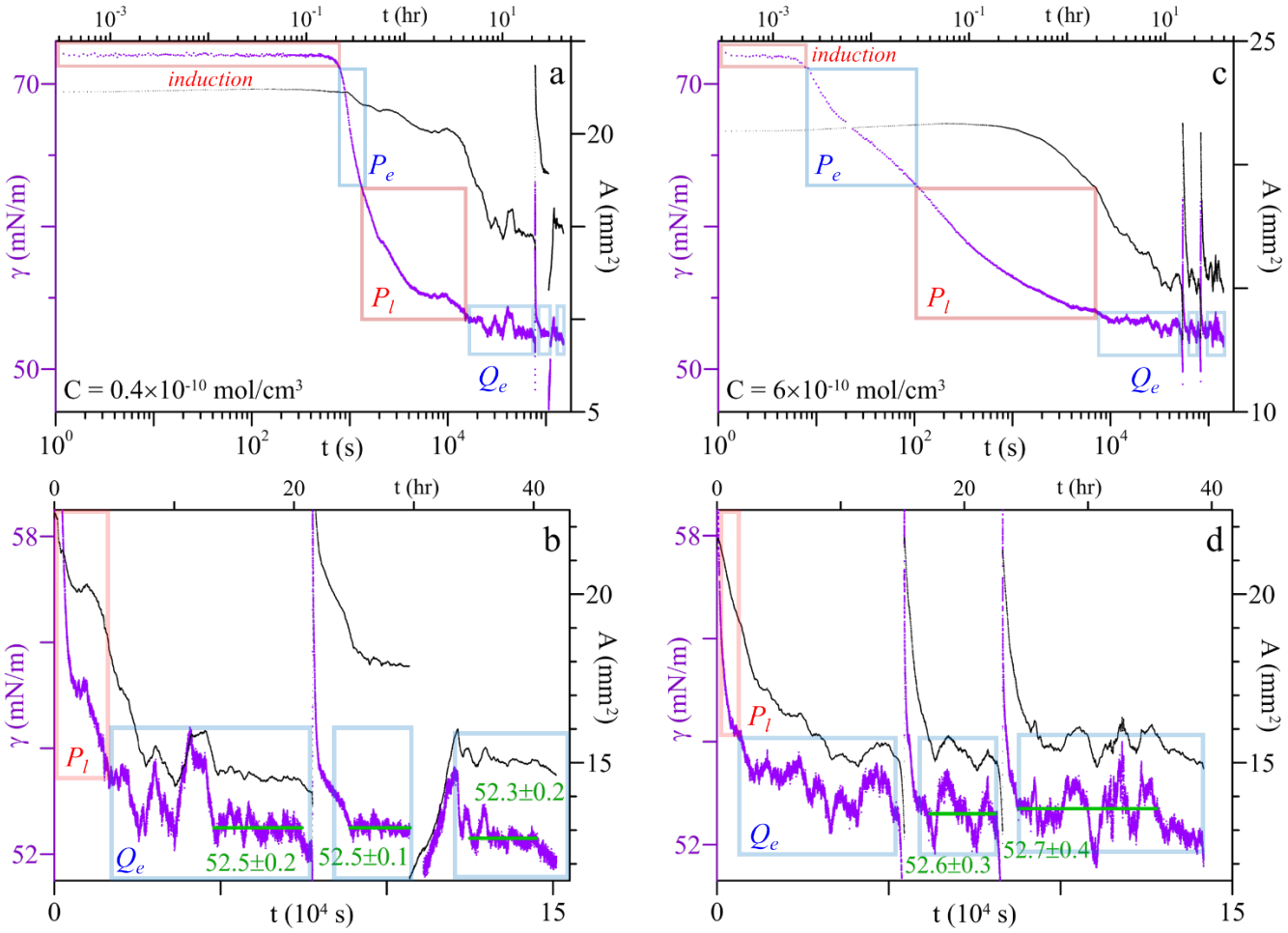

Figure S2. Relaxations of surface tension (γ) and surface area (A) of purely aqueous BSA solution and the pendant bubble, respectively, at C = 0.4 (a-b) and 6 (c-d) (10^{-10} mol/cm^3). P_e, P_l, and Q_e indicate post-induction (early, latter) and quasi-equilibrium regimes, respectively.

Similar behavior was also observed at $C_{BSA} = 6\times10^{-10}$ mol/cm^3 (Figures S2c-d). The ST initially relaxed smoothly and gradually (at t < ~2 hr, Figure S2c). Afterward, it relaxed considerably slower, eventually reaching and remaining fairly constant for a prolonged duration (at ~52.6 mN/m, Figure S2d) while fluctuating notably. Note that, the ST relaxation of BSA solution can be generally divided into three distinct regimes [21]: induction, post-induction [early (P_e), latter (P_l)], and quasi-equilibrium (Q_e), as shown in Figures S1 and S2.

S3. Average dilational modulus (E_{avg}) of adsorbed BSA film at C_{BSA} = 15×10^{-10} mol/cm^3

In general, more than 300 perturbances were identified amidst the overall SA and ST relaxations of each run. More than half of these perturbances were distinct (i.e., $\Delta A > \sim 0.05$ mm^2 and $\Delta\gamma > \sim 0.1$ mN/m) and characterized by nearly linear changes in SA and ST, as illustrated by the examples in Figures S3 and S4.

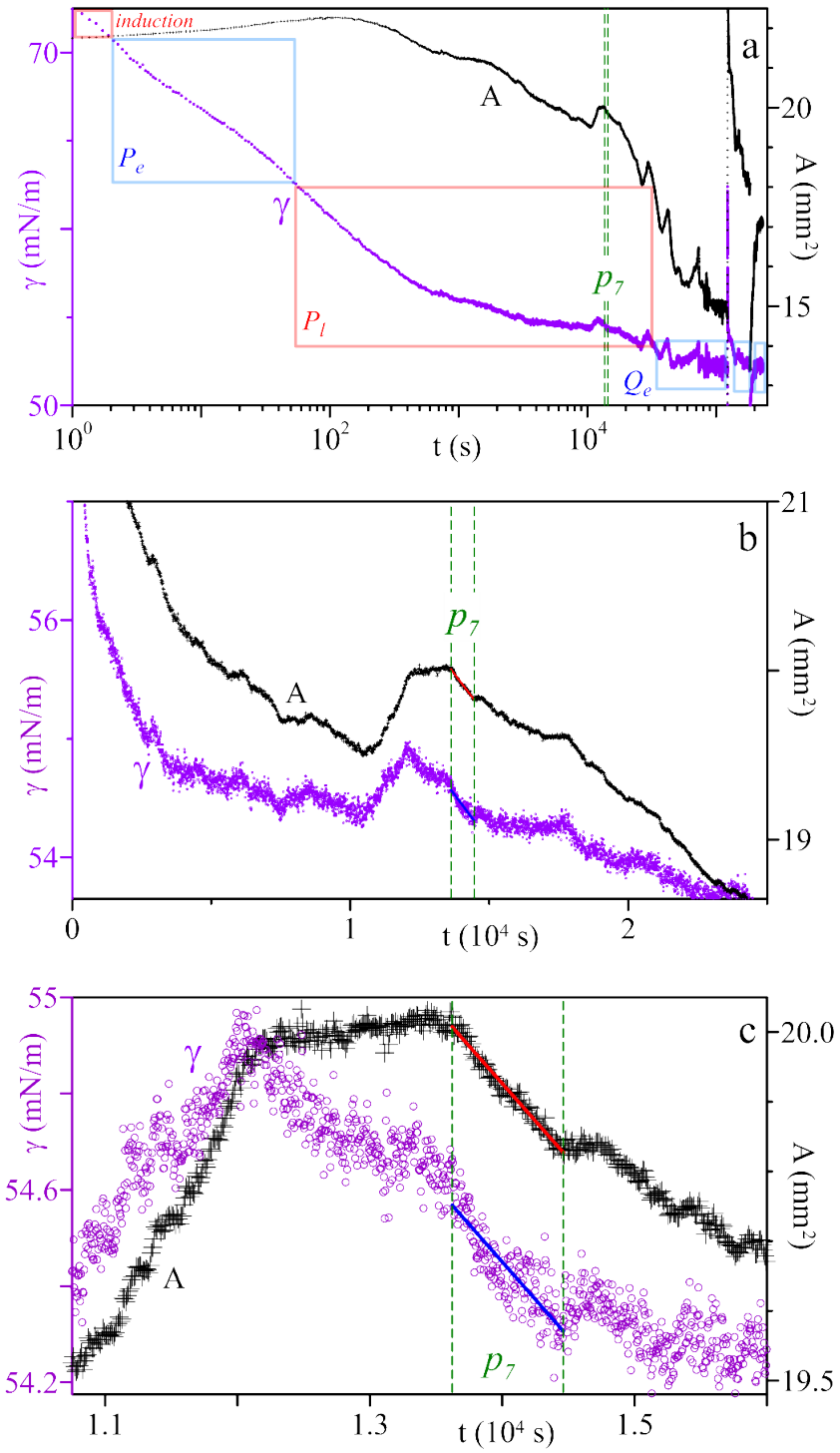

Figure S3. Relaxations of ST (γ) and SA (A) of $BSA_{(aq)}$ solution at C = 15×10^{-10} mol/cm^3, depicting a perturbance (p_7) that was identified at the latter post-induction (P_l) regime.

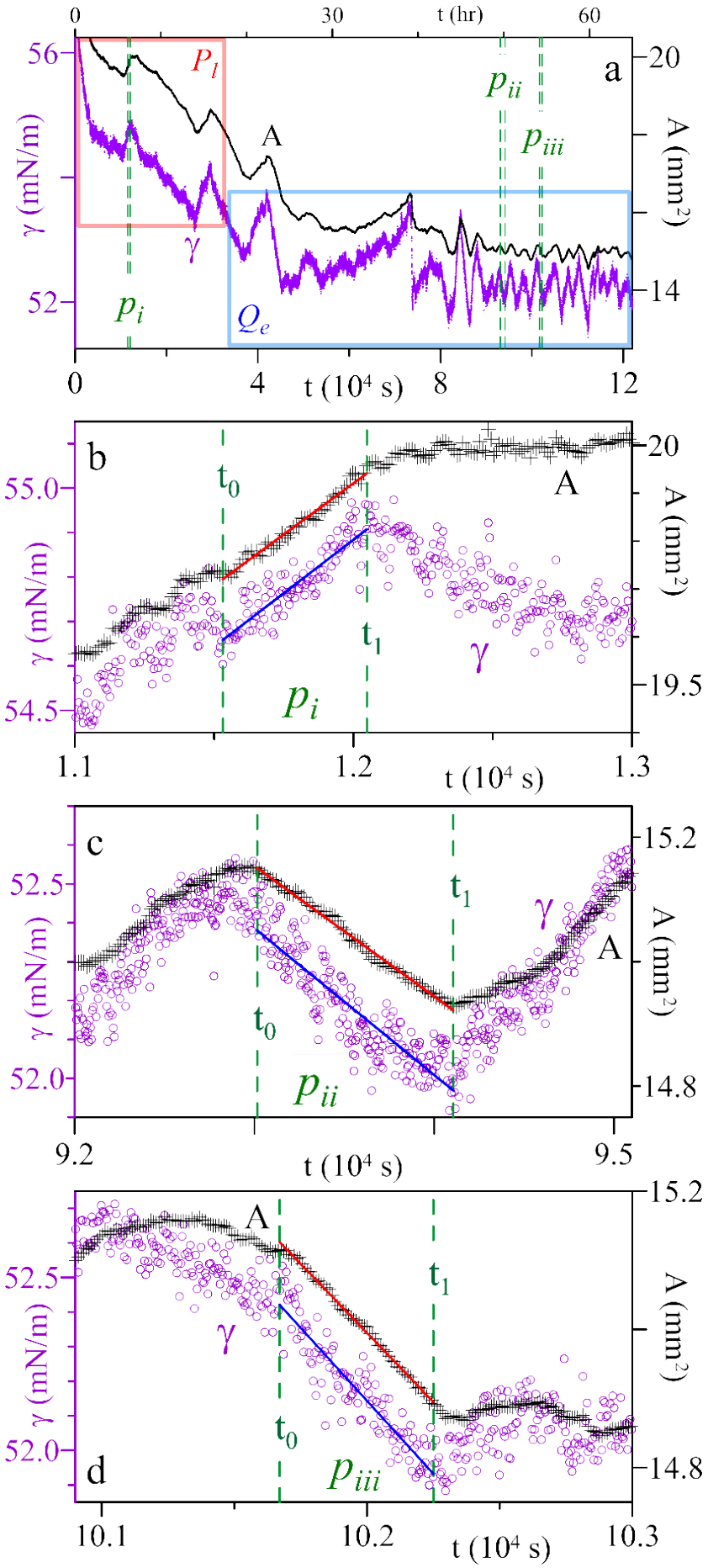

Figure S4. (a) Relaxations of ST (γ) and SA (A) of $BSA_{(aq)}$ solution, at C = 15×10^{-10} mol/cm^3, showing three perturbances identified at the post-induction (b) and quasi-equilibrium (c,d) regimes.

The dilational modulus was evaluated following the manner in ref [23]. Briefly, the onset (at t_0) and end (t_1) of each perturbance were first identified (indicated by dashed lines in Figures S3 and S4). As the ST and SA relaxed in a nearly linear manner during the perturbance, the relaxation data were best-fitted linearly to obtain $d\gamma/dt$ and dlnA/dt; then dilational modulus [$E_i = (d\gamma/dt)/(dlnA/dt)$] was calculated. The data (t_0, t_1, A_0, A_1, γ_0, γ_1, dlnA/dt, $d\gamma/dt$, and E_i) corresponding to perturbance p_7 and p_i – p_{iii} were tabulated in Table S4.

Table S4. Data pertaining to perturbances (p_7, p_i-p_{iii}) in Figure 2a, Figures S3 and S4

	t_0 (10^4 s)	t_1 (10^4 s)	A_0 (mm^2)	A_1 (mm^2)	$\Delta A/A_0$ (%)	γ_0 (mN/m)	γ_1 (mN/m)	$\Delta\gamma$ (mN/m)	dlnA/dt (10^{-5} s^{-1})	$d\gamma/dt$ (10^{-4} mN/m.s)	E_i (mN/m)
p_7	1.362	1.446	20.00	19.83	-0.90	54.57	54.31	-0.26	-1.07	-3.11	29
p_i	1.153	1.205	19.66	19.99	1.12	54.43	54.73	0.30	-1.62	-4.86	30
p_{ii}	9.308	9.414	15.15	14.92	-1.51	52.38	51.97	-0.41	-1.43	-3.90	27
p_{iii}	10.168	10.225	15.13	14.90	-1.50	52.42	51.92	0.50	-2.65	-8.40	32

Using this approach, the local dilational modulus (E_i) at a specific short region of time (t_i) was evaluated for numerous (150 – 200) distinct perturbances on each run (as denoted by circles in Figures S5a and S5c). Alternatively, the data, $d\gamma/dt$ and dlnA/dt, of several distinct perturbances, identified successively over a considerably long time range were plotted in a $d\gamma/dt$ vs. dlnA/dt plot [e.g., t = 0.04 – 0.15 and t = 9.3 – 10.5 (10^4 s); Figures S5b and S5d, respectively]. These data points were then best-fitted linearly (through the origin) to obtain the E_{avg} (the slope of this best-fitting line) over this time interval. The horizontal line in Figures S5a and S5c shows this E_{avg}.

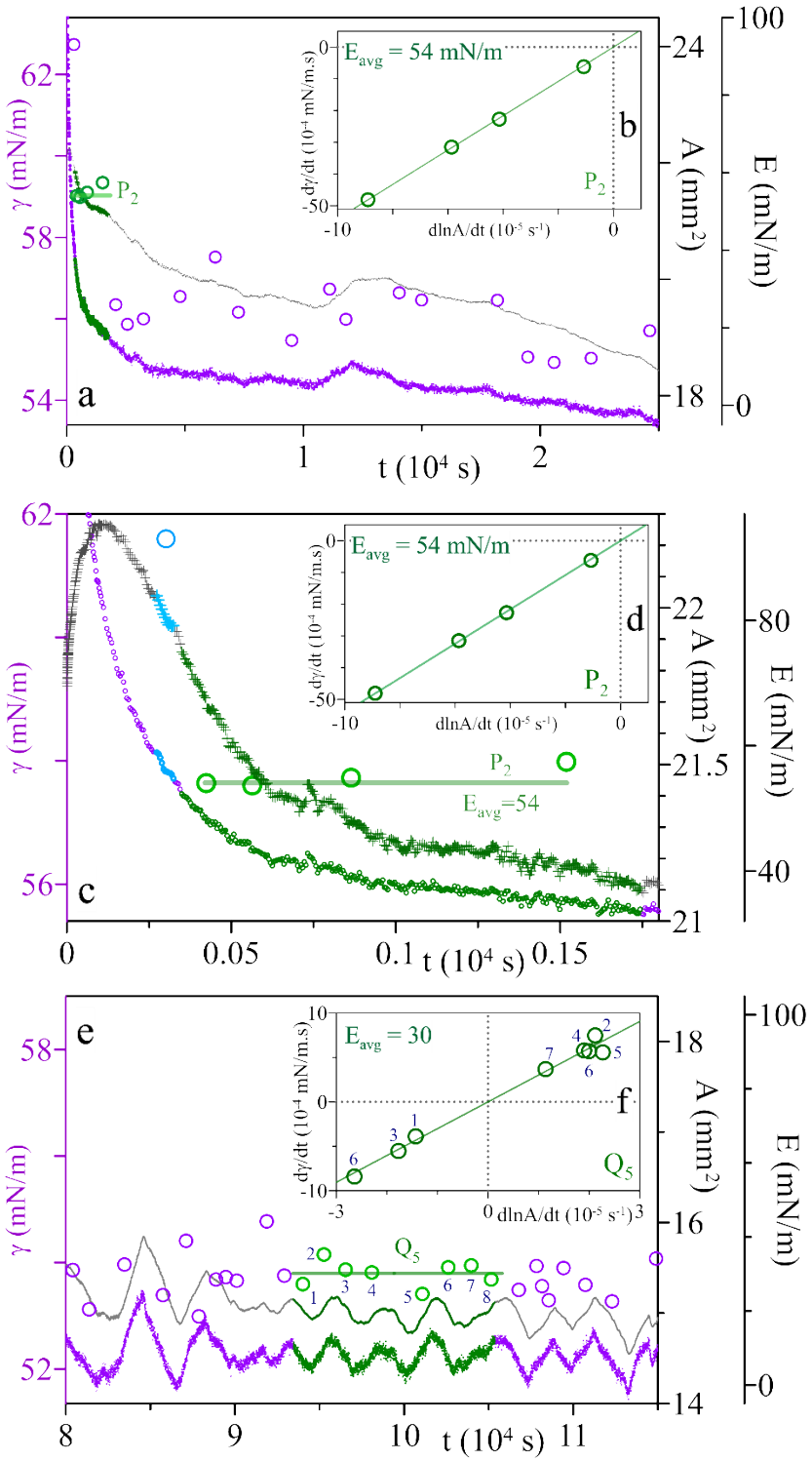

Figure S5. (a,c,e) Variation of the dilational modulus (E, ○) of an adsorbed BSA film (C_{BSA} = 15×10^{-10} mol/cm^3) as a function of time alongside the corresponding ST and SA relaxations. Dependency between the rate of ST change (dγ/dt) and relative surface expansion rate (dlnA/dt) of the perturbances (○) identified t = 0.04 – 0.15 (b,d) and t = 9.3 – 10.5 (f) (10^4 s), respectively; wherein, E_{avg} was obtained from the slope of the best-fitted line.

S4. Variation of E_{avg} of the adsorbed BSA film

When the values of E_{avg} were plotted alongside the ST and SA relaxations, as shown in Figure S6, a clear variation in E_{avg} was observed during the BSA adsorption process. The E_{avg} sharply decreased (from ~90 mN/m, green □) and reached a minimum of ~16 mN/m (red △) at the P_l regime (red O). Afterward, at the Q_e regime (blue and purple O), E_{avg} rose from this minimum, oscillated at ~30 mN/m (+) for a considerable duration, and eventually reached a relatively stable value of ~ 40 mN/m (green circles). This relatively stable E_{avg} indicates that it takes a considerably long time (> 10^5 s) for the adsorbed BSA molecules to form a saturated film, even though the ST had reached its equilibrium value a long time ago.

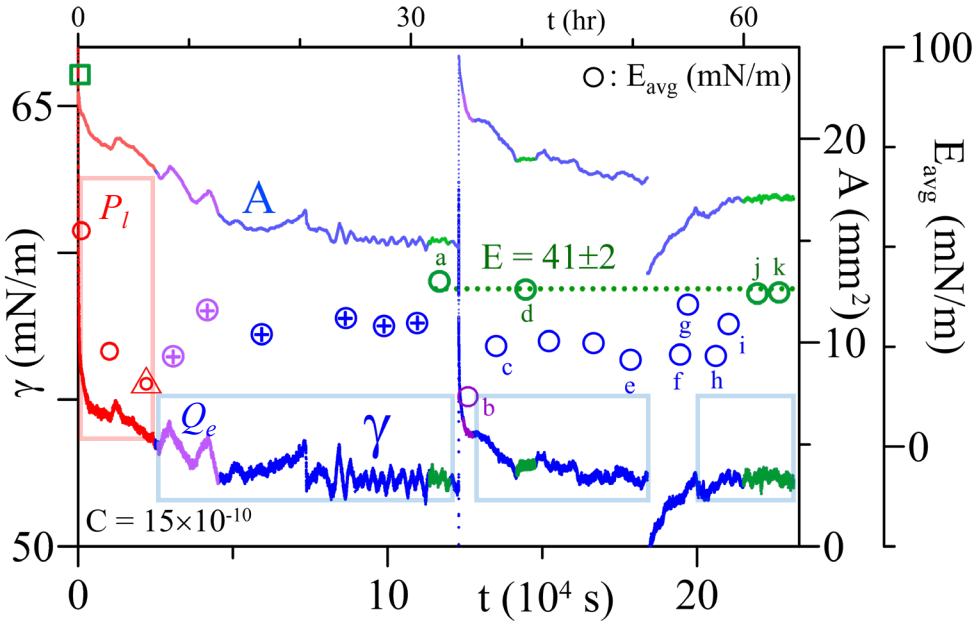

Figure S6. Variation of E_{avg} (average dilational modulus) of the adsorbed BSA film as a function of time alongside the corresponding ST (γ) and SA (A) relaxations at $C_{BSA} = 15\times10^{-10}$ mol/cm^3. P_e, P_l, Q_e refers to the post-induction (early, latter) and quasi-equilibrium regimes. The triangle (△) signifies the minimum value of E_{avg}, and the plus (+) signifies the subsequent increase and oscillation.

A similar variation in E_{avg}, during the BSA adsorption, was also observed at other BSA concentrations. Figure S7 shows another two examples at C_{BSA} = 0.4 and 6 (10^{-10} mol/cm^3): E_{avg} dropped sharply from ~ 125 mN/m, reached a minimum (15 and 17 mN/m, respectively; △), rose, oscillated for a considerable time (+), and then reached a stable E_{avg} after a significant duration (green O) at t > 10^5 s.

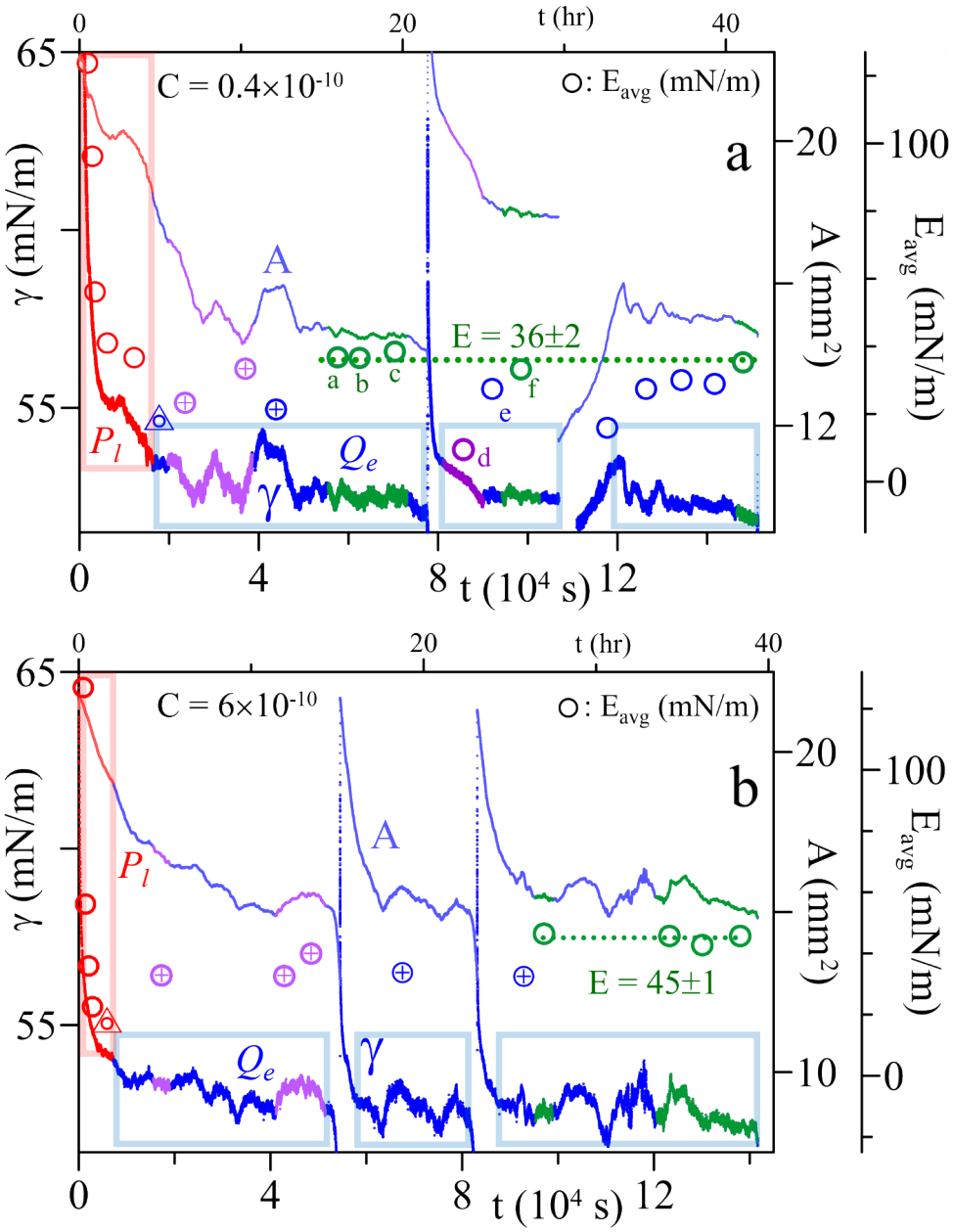

Figure S7. Variation of E_{avg} of the adsorbed BSA film as a function of time alongside the corresponding ST (γ) and SA (A) relaxations at C_{BSA} = 0.4 (a) and 6 (b) (10^{-10} mol/cm^3). P_e, P_l, Q_e refers to the post-induction (early, latter) and quasi-equilibrium regimes. The triangle (△) signifies the minimum value of E_{avg}, and the plus (+) signifies the subsequent increase and oscillation.

S5. Time taken for the adsorbed BSA film to reach a saturated state

There is limited information in the literature on the time needed for an adsorbed film to reach its saturated state. How long did it take for an adsorbed BSA film in this study to reach a saturated state? The time needed to reach saturation (t_{sat}) was estimated from the variation in E_{avg} at C_{BSA} = 0.05 – 60 (10^{-10} mol/cm^3) (Figures S6 and S7): (i) the time range for the earliest stable E_{avg} detected, corresponding to a saturated absorbed film, was identified; and (ii) the ST and SA relaxations within the time interval covered by this E_{avg} was examined. The t_{sat} = 27 – 40 hours [9.7 – 14.5 (10^4 s), averaging at ~35 hours] (shown in Figure S8). This t_{sat} is much longer than the film's lifetime (t_{life}) in the literature for BSA (0.05 – 24 hrs, Table S2b); thus, suggesting that the reported *E* values were likely not that of a saturated film.

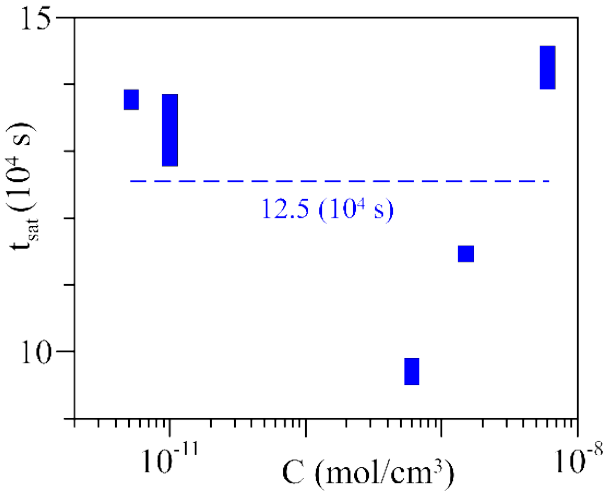

Figure S8. Estimated time taken for the adsorbed BSA film to reach its saturated state (t_{sat}) at varying C_{BSA}. The horizontal bars represent the time range for earliest stable E_{avg} detected.

The t_{sat} was also compared to the time needed to reach the equilibrium ST. Figure S9 illustrates an example at C_{BSA} = 15×10^{-10} mol/cm^3: the equilibrium ST was reached in ~21 hours, which was much shorter than the t_{sat} (~32 hours). This likely suggested that despite reaching the equilibrium ST, an adsorbed BSA film might require a longer time to rearrange in order to reach its saturated state. However, further study is needed for confirmation.

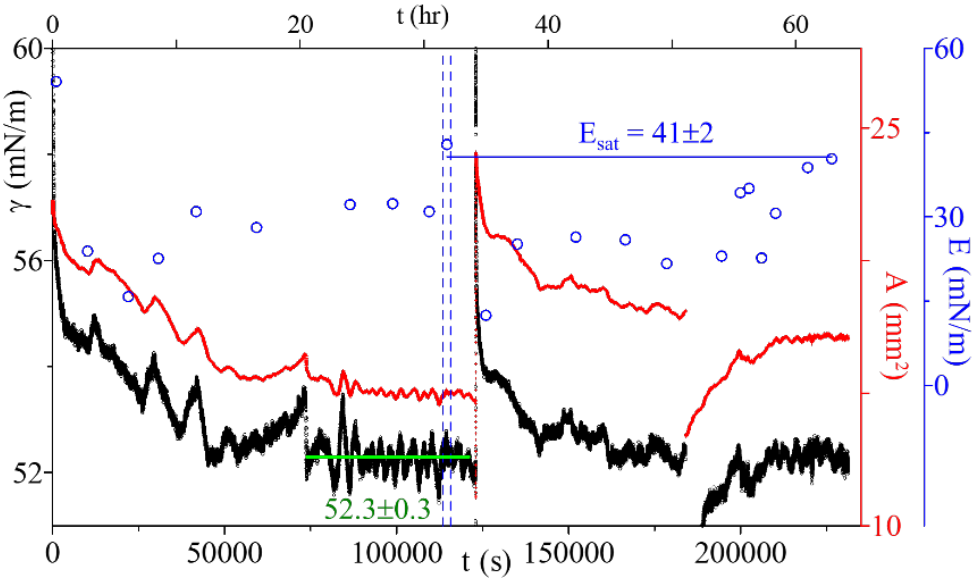

Figure S9. Variation of E_{avg} of the adsorbed BSA film as a function of time alongside the corresponding ST (γ) and SA (A) relaxations at $C_{BSA} = 15\times10^{-10}$ mol/cm^3. The vertical dashed lines indicate the t_{sat}.

S6. Effect of rapid surface perturbation

At the Q_e (quasi-equilibrium) regime, some large, forced perturbations (rapid compression/expansion of the pendant bubble) were conducted to (i) verify if the ST relaxed back to its previous value and (ii) evaluate how E_{avg} would be affected by such rapid surface perturbations. Figure 5 illustrates an example at C = 15×10^{-10} mol/cm^3: when the pendant bubble was subjected to a forced perturbation (initial ~25% SA decrease in ~0.7 s, then abrupt 116% increase in ~5 s; Figure S10), E_{avg} sharply dropped from ~40 (of the saturated film) to ~13 mN/m; then, it rose steadily, approached and reached the previous ~40 mN/m.

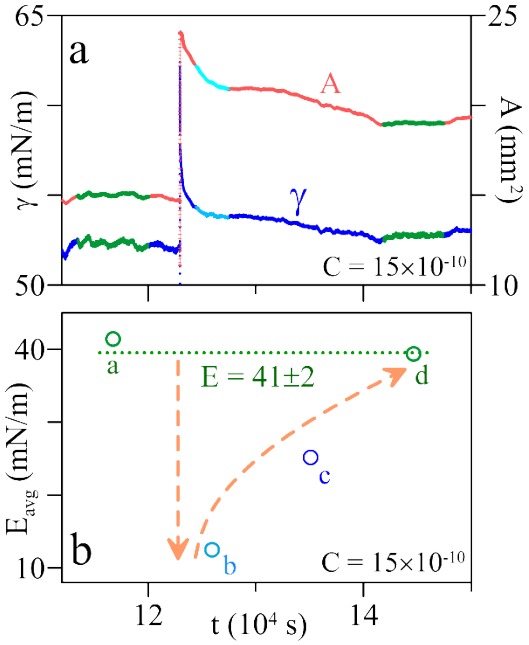

Figure 5 (in manuscript**).** (a) Relaxations of ST (γ) and SA (A) at C_{BSA} = 15×10^{-10} mol/cm^3, during a rapid perturbation (compression-expansion) of the pendant bubble and (b) the corresponding variation of E_{avg} of the adsorbed BSA film as a function of time. The labels' a-d' signifies the E_{avg} values in Figure 3 (of the manuscript).

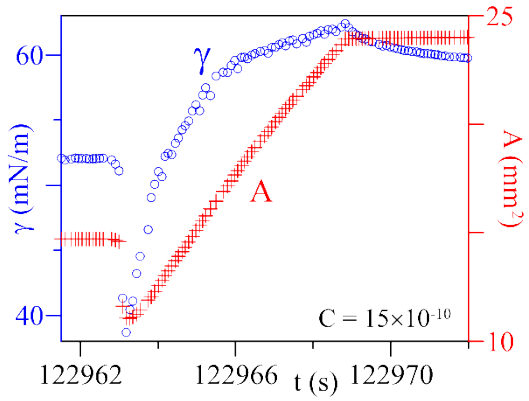

Figure S10. Relaxations of ST (γ) and SA (A) of $BSA_{(aq)}$ (at C = 15×10^{-10} mol/cm^3) during a rapid perturbation (compression-expansion) of the pendant bubble.

Similar behavior was also observed at other C_{BSA}: an additional example at $C_{BSA} = 0.4\times10^{-10}$ mol/cm^3 is shown in Figures S11 and S12. When the pendant bubble was subjected to a forced perturbation (initial ~30% SA decrease in ~0.5 s, then abrupt 144% increase in ~6 s; as shown in Figure S11), E_{avg} sharply dropped from ~36 (of the saturated film, Figure S12) to ~10 mN/m; then, it rose steadily, approached and reached the previous ~36 mN/m. This big decrease and the subsequent slow increase in E_{avg} may indicate a breakage [25,26] and recovery [27, 28] of the adsorbed BSA film.

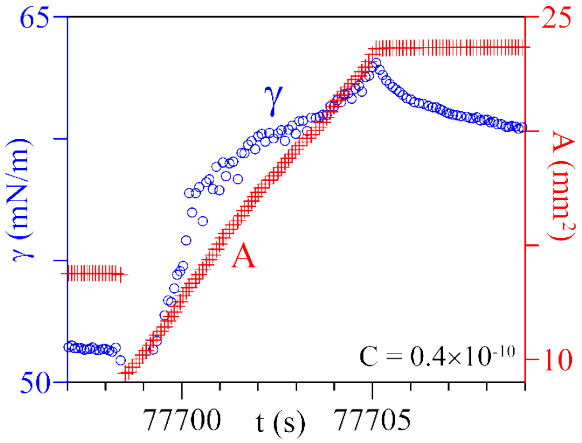

Figure S11. Relaxations of ST (γ) and SA (A) of $BSA_{(aq)}$ (at $C = 0.4\times10^{-10}$ mol/cm^3) during a rapid perturbation (compression-expansion) of the pendant bubble.

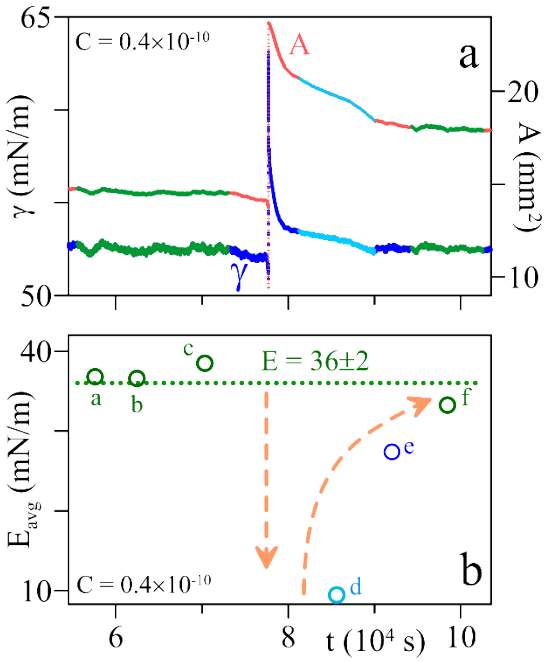

Figure S12. (a) Relaxations of ST (γ) and SA (A) of $BSA_{(aq)}$, at $C = 0.4\times10^{-10}$ mol/cm^3, during a rapid perturbation (compression-expansion) of the pendant bubble and (b) the corresponding variation of E_{avg} of the adsorbed BSA film as a function of time. The labels' a-f' signifies the E_{avg} values in Figure 4a (of the manuscript).

S7. E_{avg} at the early stage of BSA adsorption

The E_{avg} was obtained by plotting the dγ/dt vs. dlnA/dt of several distinct perturbances identified successively over a considerably long time (previously detailed in Section S3 and illustrated in Figure S5). When these E_{avg} were plotted alongside the ST and SA relaxations, a clear variation in E_{avg} was observed during the BSA adsorption process. For instance, at $C_{BSA} = 15\times10^{-10}$ mol/cm^3 (Figure 3), E_{avg} initially exhibited a sharp decrease (from > 90 mN/m) and reached a minimum (~16 mN/m); afterward, it rose and oscillated for a considerable time before eventually reaching a E_{avg} value of a saturated BSA film after a significant duration.

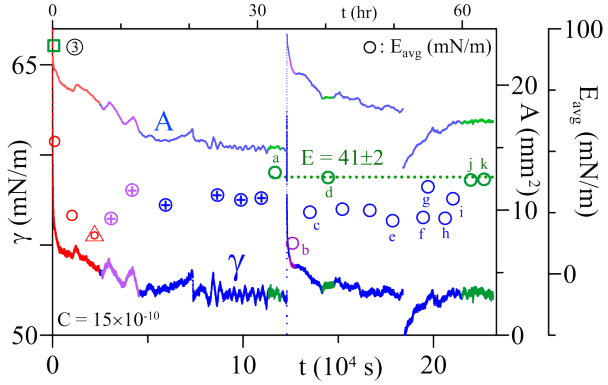

Figure 3 (in manuscript**).** Variation of E_{avg} (average dilational modulus) of the adsorbed BSA film as a function of time alongside the corresponding ST (γ) and SA (A) relaxations at $C_{BSA} = 15\times10^{-10}$ mol/cm^3. The triangle (△) signifies the minimum value of E_{avg}, and the plus (+) signifies the subsequent increase and oscillation.

For the run at $C_{BSA} = 15\times10^{-10}$ mol/cm^3, the first E_i value was obtained from relaxation data of the first perturbance (that was somewhat distinct, whose change in ST was in harmony with the SA change) identified amidst the overall ST and SA relaxations in the P_l regime (t = 131 ~157 s, Figure S13). The E_{avg} obtained from the first three identifiable perturbances are shown in Figure S14b and Table S5 with a large variation: 260, 143, and 93 mN/m, with an average of 173 mN/m. These E_{avg} are much larger than the E_{avg} for a saturated BSA film (E_{avg} = 41 mN/m, at C = 15×10^{-10} mol/cm^3).

Till now, the contribution of the BSA adsorption at the P_l regime during a perturbance is unknown. However, at the Q_e regime, the ST kept reasonably constant, and it is likely that the contribution of the BSA adsorption/desorption on the Δγ (change in ST) during the perturbance was negligible. The big E_{avg} for perturbances ①②③ was likely not real, but due to the significant contribution of BSA adsorption (which caused a significant decrease in ST) during the P_l regime. This is why the first two perturbances ①② were not included in the manuscript.

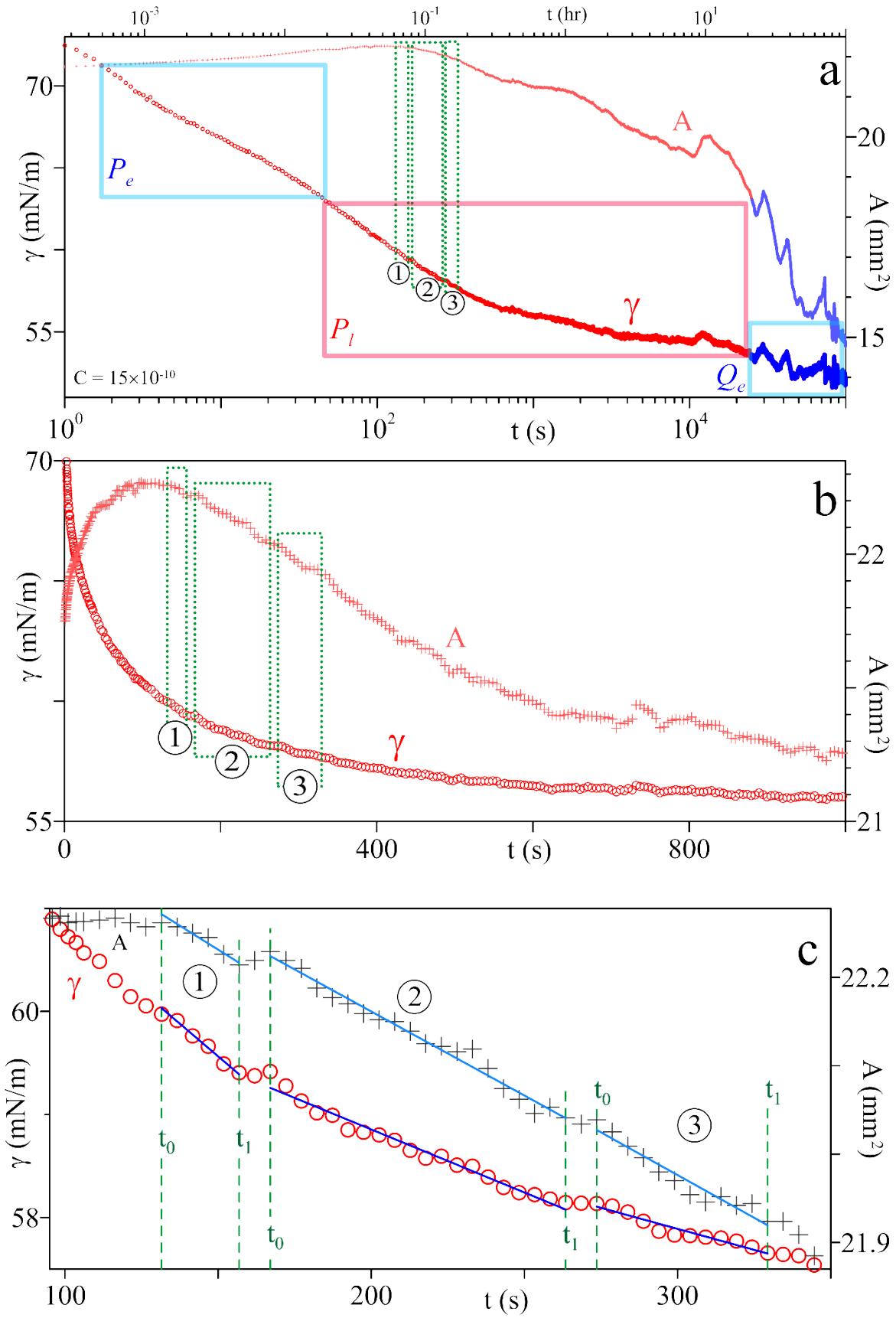

Figure S13. Relaxations of ST (γ) and SA (A) of a $BSA_{(aq)}$ solution at C = 15×10^{-10} mol/cm^3, showing the first three identifiable perturbances (①②③) at the latter post-induction regime. P_e, P_l, Q_e refers to the post-induction (early, latter) and quasi-equilibrium regimes.

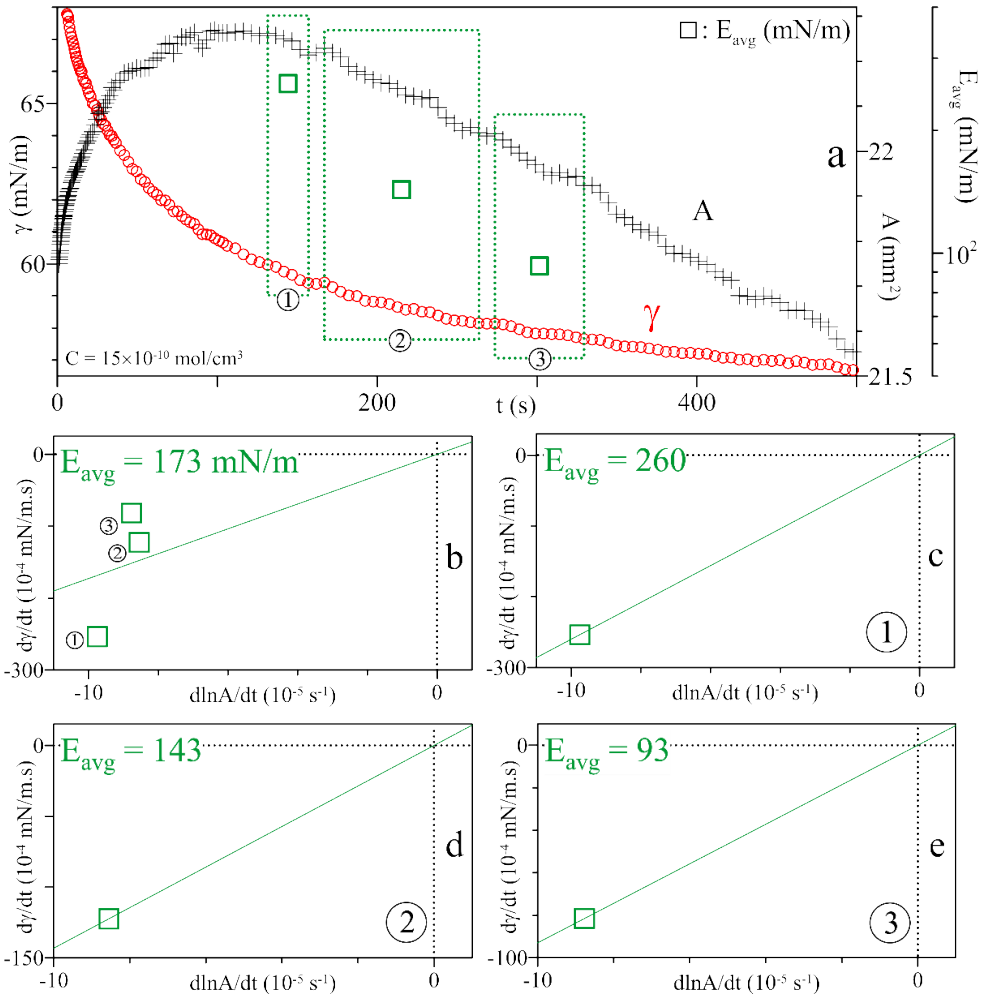

Figure S14. (a) Variation of E_{avg} of the adsorbed BSA film (C_{BSA} = 15×10^{-10} mol/cm^3) as a function of time alongside the corresponding ST (γ) and SA (A) relaxations. (b-d) Dependency between the rate of ST change (dγ/dt) and relative surface expansion rate (dlnA/dt) of the perturbances (○) identified at t = 130 – 330 s; wherein, E_{avg} was obtained from the slope of the best-fitted line.

Table S5. Data pertaining to the perturbances ① – ③ in Figure S12

	t_0 (s)	t_1 (s)	A_0 (mm^2)	A_1 (mm^2)	$\Delta A/A_0$ (%)	γ_0 (mN/m)	γ_1 (mN/m)	$\Delta\gamma$ (mN/m)	dlnA/dt (10^{-5} s^{-1})	dγ/dt (10^{-4} mN/m.s)	E_i (mN/m)
1	131	157	22.26	22.21	-0.22	60.03	59.40	0.63	-9.75	-253.6	260
2	166	262	22.24	22.05	-0.83	59.26	58.08	-1.18	-8.55	-122.4	143
3	273	329	22.03	21.92	-0.49	58.11	58.08	-0.46	-8.77	-81.6	93

The E_{avg} values reported in the manuscript (e.g., $P_{1\text{-}3}$ and $Q_{1\text{-}2}$, Figures S15b-i, at latter P_l and Q_e regime) have much higher reliability, as they were obtained from the data of multiple perturbances and a good linear relationship was observed on dγ/dt vs. dlnA/dt. This behavior was also occurred at other C_{BSA}; an additional example at C_{BSA} = 6×10^{-10} mol/cm^3 is given in Figure S16, in which, the E_{avg} varied from 549, 413, 227, 127,56, 36, 23, 16, and 32 mN/m.

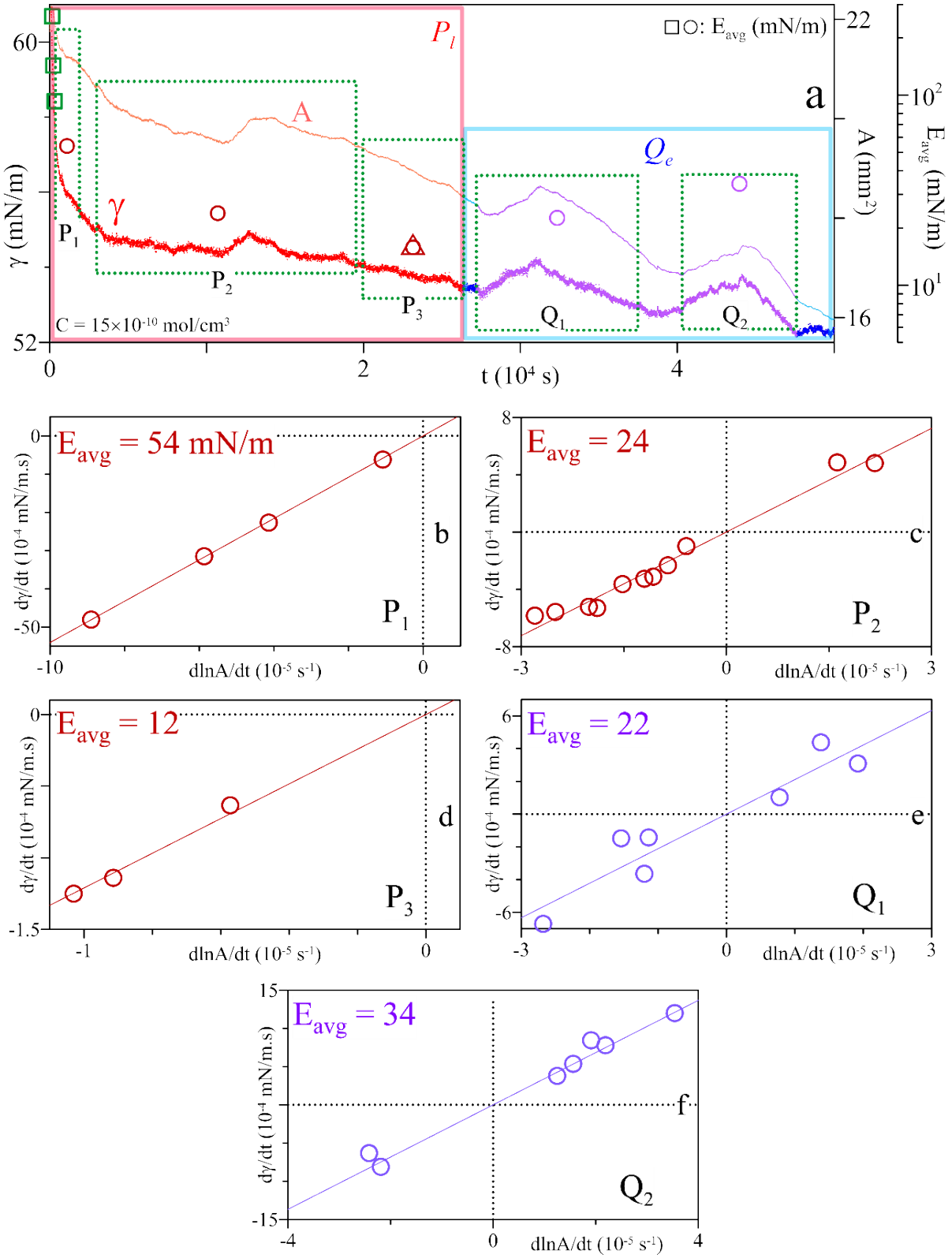

Figure S15. (a) Variation of E_{avg} of the adsorbed BSA film (C_{BSA} = 15×10^{-10} mol/cm^3) as a function of time alongside the corresponding ST (γ) and SA (A) relaxations. (b-f) Dependency between the rate of ST change (dγ/dt) and relative surface expansion rate (dlnA/dt) of those perturbances (○) identified at t = 0.01 – 4.5 (10^4 s); wherein, E_{avg} was obtained from the slope of the best-fitted line. P_I and Q_e labels refer to the post-induction (latter) and quasi-equilibrium regimes.

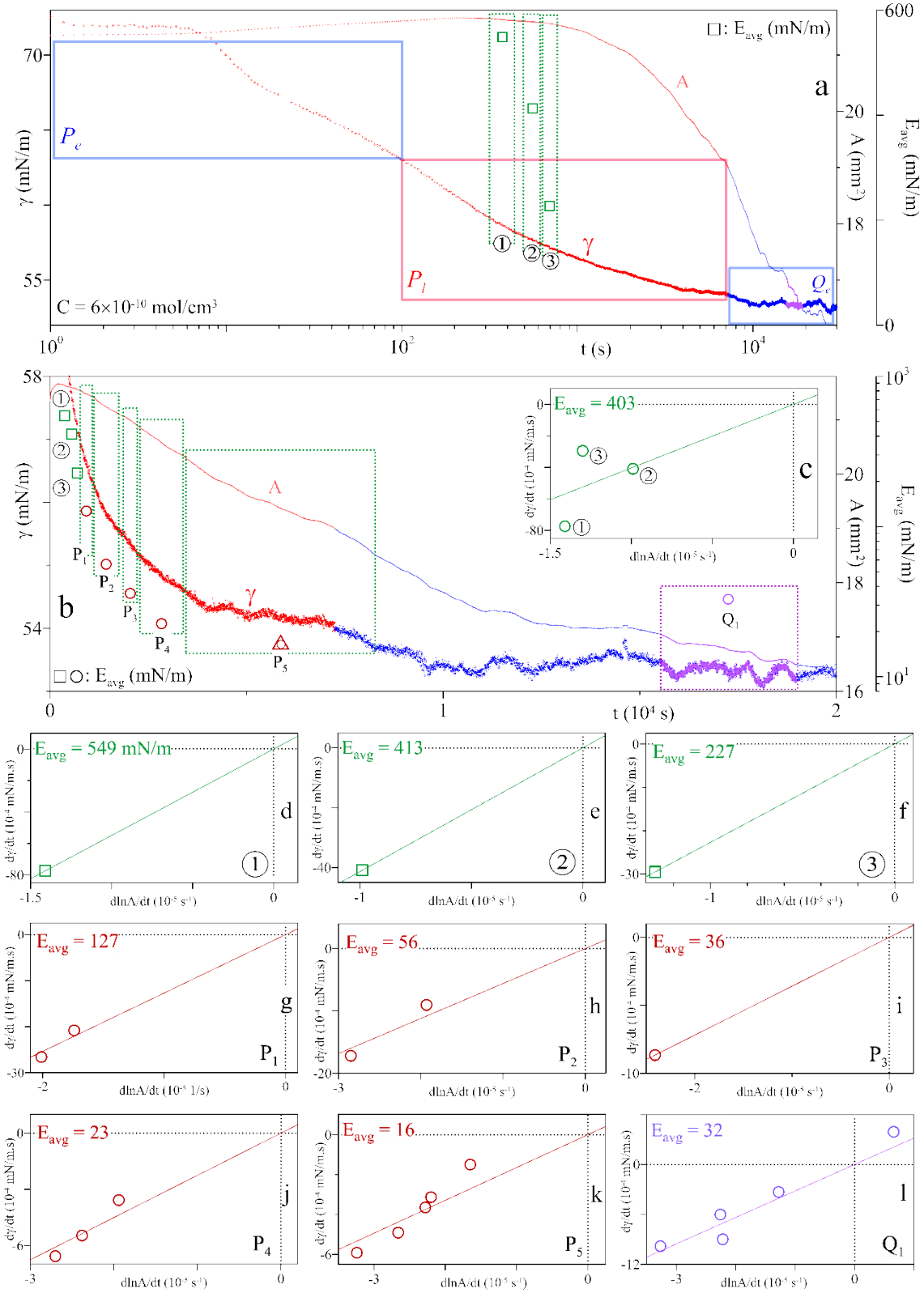

Figure S16. (a,b) Variation of E_{avg} of the adsorbed BSA film ($C_{BSA} = 6\times10^{-10}$ mol/cm^3) as a function of time alongside the corresponding ST (γ) and SA (A) relaxations. (c-l) Dependency between the rate of ST change (dγ/dt) and relative surface expansion rate (dlnA/dt) of the perturbances (○) identified at t = 0.03 – 2.0 (10^4 s); wherein, E_{avg} was obtained from the slope of the best-fitted line. The labels P_e, P_l, and Q_e refer to the post-induction (early and latter) and the quasi-equilibrium regimes.